

See discussions, stats, and author profiles for this publication at: <https://www.researchgate.net/publication/231644525>

Structural Evolution and Photoluminescence of Zinc-Blende CdSe-Based CdSe/ZnS Nanocrystals

ARTICLE *in* THE JOURNAL OF PHYSICAL CHEMISTRY C · JULY 2010

Impact Factor: 4.77 · DOI: 10.1021/jp100442v

CITATIONS

25

READS

37

5 AUTHORS, INCLUDING:



Xing Xia

Hunan University

13 PUBLICATIONS 308 CITATIONS

[SEE PROFILE](#)



Yuebin Li

Hubei University

21 PUBLICATIONS 330 CITATIONS

[SEE PROFILE](#)

Structural Evolution and Photoluminescence of Zinc-Blende CdSe-Based CdSe/ZnS Nanocrystals

Xing Xia, Zuli Liu,* Guihuan Du, Yuebin Li, and Ming Ma

School of Physics, Huazhong University of Science and Technology, 1037 Luoyu Road, Wuhan 430074, People's Republic of China

Received: January 16, 2010; Revised Manuscript Received: July 8, 2010

Anisotropic heterostructures are of significant importance in creating novel nanomaterials and realizing their application potentials. Here we report a study on structural evolution and photoluminescence of zinc-blende CdSe-based CdSe/ZnS core/shell nanocrystals with variations of the ZnS shell growth. When raising the shell growth temperature, the structure of CdSe/ZnS can be tuned from sphere to near triangle, and to branched ones, including a tetrapod-like structure. But fast interface diffusion and alloying at high growth temperature will corrupt the branched structure and induce a blue shift in the luminescence spectrum. For tetrapod-like CdSe/ZnS nanocrystals, the growth of ZnS exhibits a pattern of first elongating and then branching, which is accompanied by rising, steady, and descending phases of the photoluminescence quantum yield. This study shows the shape tuning and interface alloying of CdSe/ZnS nanocrystals, and reveals that a moderate growth temperature is necessary for obtaining tetrapod-like CdSe/ZnS nanocrystals.

1. Introduction

Heterostructured nanocrystals (NCs) have received great attention in nanomaterial research for the past decade because of their unique and superior properties and the correlated underlying mechanism.¹ For semiconductor nanomaterials, they have been manufactured into different heterostructures beside commonly obtained spheres, such as rods,² triangles,³ cubes,⁴ tetrapods,⁵ and even multibranched⁶ structures. The two naturally existing crystal structures of wurtzite (WZ) and zinc-blende (ZB) of semiconductor materials have been utilized to manipulate particle structure of semiconductor NCs, for example,^{2,5,7} nanorods are obtained by restricted growth of WZ crystal along its *c*-axis, and nanotetrapods are usually achieved by growing four arm-like WZ rods on a ZB core, which is a polytypism case that contains both WZ and ZB structures within one single particle.

The tetrapod NCs were first obtained as single component NCs, for example CdTe and CdSe, by delicately balancing the reaction parameters to achieve separate nucleation and growth stages in one reaction, in which the growth of NCs started with ZB nuclei and grew in a WZ manner.⁸ Recently, a seeded growth technique of preparing tetrapod NCs was proposed to conduct the growth of core and branched shell in two independent reactions;^{7,9} multicomponent core/shell tetrapods such as CdSe/CdS, ZnTe/CdTe, and ZnTe/CdSe were successfully obtained with this technique. Similar to conventional spherical (or near spherical) core/shell NCs, these tetrapod core/shell NCs show enhanced photoluminescence quantum yield (PL QY), and stabilities. Besides that, the out stretching arms of the tetrapod can act as antennas for light harvesting, and the energy transfer in tetrapod NCs is proven to be efficient, thus they can be very useful in applications of photovoltaic devices like light concentrators, solar cells, and LEDs.^{6a,7,10}

Among various core–shell combinations of semiconductor NCs prepared in a colloidal system, CdSe–ZnS has been the

most inviting pair because of the superior PL QY, and PL durability within CdSe/ZnS core/shell NCs, which enable CdSe/ZnS a preferred choice among various types of core/shell NCs in applications, especially as fluorescent markers in biomedical research. On the other hand, despite the fact that shape tuning has been realized in many types of single- and multicomponent NCs,^{2–11} the structure of CdSe/ZnS NCs still basically remains a “dot”, and a very limited amount of research work has reported the shape variation of CdSe/ZnS by means of chemical vapor deposition.¹² The shell component ZnS of CdSe/ZnS NCs is one of the most important and extensively adopted materials in phosphors due to its ~3.6 eV band gap energy, which is the widest among similar II–VI semiconductors such as CdSe, CdS, ZnTe, ZnSe, and ZnO. Hence, structural diversity of CdSe/ZnS NCs may offer opportunities to further explore this important heterostructured material, and facilitate its applications in the photovoltaic realm.

In this article, we show the structural evolution of CdSe/ZnS synthesized using the colloidal chemical method in addition to commonly obtained spherical quantum dots. Shape evolvement was studied by conducting a series of experiments with growth temperature of ZnS ranging from 180 to 280 °C, and the corresponding optical properties were analyzed. Then, the tetrapod-like CdSe/ZnS NCs discovered in the shape tuning research were further studied by altering the amount of ZnS precursor, i.e., to adjust the length of ZnS arms; structural and optical properties of these branched NCs were also discussed.

2. Experimental Section

2.1. Chemicals. Cadmium oxide (CdO, 99%, Damao Chemical Co.), selenium shot (Se, 99.99%, Strem Chemicals), sulfur powder (S, 99%, Aidehua Development Co.), zinc oxide (ZnO, 99%, Sinopharm Chemical Reagent Co./SCR), stearic acid (SA, SCR), oleic acid (OA, tech. grade, Alfa Aesar), octadecylamine (ODA, 95%, Fluka), rhodamine 6G (99%, Acros), and 1-octadecene (ODE, 90%, Aldrich) were used as received without

* To whom correspondence should be addressed. E-mail: zliu@mail.hust.edu.cn. Phone: +86-27-8755-6264. Fax: +86-27-8755-6264.

further processing. All solvents including methanol, chloroform, hexane, and acetone were of analytical grade and purchased from SCR.

2.2. Synthesis of Nanocrystals. ZB CdSe NCs were synthesized by adopting a newly developed noninjecting method where a fast injection of precursor solution is not required.¹³ Briefly, 0.2 mmol of CdO was first dissolved with 0.17 g of SA at 200 °C, and then 10 mL of ODE and 0.4 mmol of Se were added, and the mixture was heated to 240 °C under argon for growing CdSe. When the mixture turned from colorless to red, 2 mL of 0.1 M Cd stock solution (prepared by dissolving CdO with OA and ODE at ~280 °C) was introduced in a stepwise manner at a rate of ~0.67 mL/min to promote further growth of CdSe NCs and improve their solubility. The heating was stopped when the mixture turned deep red, then CdSe NCs were purified and collected.

The growth of ZnS shell was carried out with the Successive Ion Layer Adsorption and Reaction (SILAR) technique,¹⁴ which had imitated the atomic-layer-epitaxy of Molecular Beam Epitaxy by growing shells with alternative adsorptions of cation and anion in a colloidal reaction system. Before the experiments, 0.1 M Zn and S precursor solutions were prepared, respectively, and the amount of precursor solution needed for generating one monolayer of ZnS was calculated. A detailed description of this procedure is given in the Supporting Information. For the experiments with varying temperature, 1.5 mL of CdSe hexane solution containing $\sim 1 \times 10^{-4}$ mmol of CdSe particles, 5 mL of ODE, and 2 g of ODA were loaded together into a flask, which was pumped to remove hexane and flushed with argon. Then the flask was heated to the desired temperature (180, 200, 220, 240, 260, and 280 °C) and a calculated amount of Zn precursor solution was injected, followed by incubation for 15 min, and then an injection of S precursor was given to grow the first monolayer of ZnS. The shell thickness was designed to be 8 monolayers (MLs) despite the shape of the final product, and the time interval between two injections was set as 15 min. The rest of the monolayers of ZnS were grown by further injecting Zn and S precursors accordingly.

In the series of experiments altering the amount of ZnS, the procedures were similar, except that the reaction temperature was fixed at 240 °C and the ZnS shell was designed to alter from 2 to 16 MLs. Thus 32 injections were applied for the final product with 16 MLs of shell. To avoid dilution of the reaction mixture induced by multiple precursor injections, the whole experiment was divided into three reaction parts that respectively grew ZnS shell from 1 to 6 MLs, 7 to 12 MLs and 13 to 16 MLs. NCs were purified and collected after each reaction part, and reloaded for the following experiments. Portions of NCs with 2, 4, 6, 8, 12, and 16 MLs of ZnS were kept for characterizations.

2.3. Measurements. Transmission electron microscopy (TEM) and high resolution TEM (HRTEM) were performed respectively on a Tecnai G² 20 and a Tecnai G² FT20 transmission electron microscope (FEI Company) with acceleration voltage of 200 kV. Electron Energy Loss Spectroscopy (EELS) was performed for elemental mapping on HRTEM equipped with a Gatan GIF 2001 image filter. The TEM samples were prepared by dropping diluted solutions of NCs on copper grids covered with amorphous carbon film; ultrathin carbon film (~5 nm) covered copper grids were adopted for HRTEM observation. Absorption spectra were obtained with a Lambda 25 UV-vis spectrometer (PerkinElmer Inc.) using standard 1 cm × 1 cm quartz cells. PL spectra were obtained with an FP-6500 fluorescence spectrometer (JASCO Inc.). Photoluminescence

quantum yield was calculated with reference to ethanol solutions of rhodamine 6G; in the spectral measurement, all samples were excited at a wavelength of 480 nm, where the movements of their absorption curves were in plateau slopes, and the optical densities were kept around 0.05.¹⁵ Powder X-ray diffraction (XRD) was performed on an X'Pert Pro X-ray diffractometer (PANalytical B.V.) with Cu K α rotating anode source and generator settings at 40 kV and 40 mA. XRD samples were prepared by dropping concentrated NCs solutions on glass slides that were allowed to dry in air.

3. Results and Discussion

3.1. Effect of ZnS Growth Temperature. The effect of ZnS growth temperature was studied by coating CdSe with 8 MLs of ZnS at different temperatures ranging from 180 to 280 °C. The results show that temperature affects not only the morphologies and structures of resulting NCs, but also their optical properties.

Figure 1 shows the structural evolution of CdSe/ZnS NCs prepared at different ZnS growth temperatures. The ZB CdSe NCs in Figure 1a appear to be “dot” shaped particles, and the shape does not change much after coating with ZnS at 180 °C (Figure 1b). But from 200 °C and above, a tendency of oriented shell growth occurs and it causes branching of ZnS. The NCs exhibit near triangular shape when grown at 200 °C (Figure 1c), branched shape at 220–260 °C (Figures 1d–f), and corrupted branched shape at 280 °C (Figure 1g). Figure 1h gives a schematic view of this structural evolution.

In Figure 1c, the near triangular shape of NCs under TEM implies a pyramidal tetrahedron structure, which means that the ZnS growth is already facet oriented at 200 °C. Panels d–f of Figure 1 further demonstrate this selective shell growth fashion, that the ZnS shell becomes no longer the commonly assumed covering coating, but grows into out stretching arm-like rods. Some particles show tribranched morphology, which is a character of tetrapod that each particle has three rods to support its standing, and the other rod usually stretches upward, hence is not obvious under TEM. From the widely accepted growth mechanism of tetrapod NCs, the shell material usually grows in WZ phase along its *c*-axis on four (111) surface facets of a ZB core.^{5,7,9} Thus, in our experiment the crystal structure of the ZnS arms can be anticipated to be WZ. Figure 1g shows that when the growth temperature is further increased to 280 °C the branched structure is corrupted, exhibiting very rough particle shape. It is apparent that in Figure 1e most particles have tetrapod-like structure with symmetric and narrow ZnS arms, while in Figure 1f the particles turn out to be asymmetric, indicating that 260 °C is already too high for the growth of tetrapod-like CdSe/ZnS.

For anisotropic heterostructured NCs obtained by colloidal chemical methods, even though branched or tetrapod shape has been realized in many types of single- and multi-component materials, to the best of our knowledge, colloidal branched CdSe/ZnS NCs have not been reported yet. We think this can be ascribed to the fact that the structure of branched CdSe/ZnS is highly sensitive to the shell growth temperature. Our experiment has revealed that 260 °C is already inappropriate for preparing tetrapod-like CdSe/ZnS, whereas other types of core/shell tetrapods such as CdSe/CdS, ZnTe/CdTe, and CdSe/CdTe were reported to be grown at above 300 °C.^{7,9b} The WZ crystal structure of ZnS is a metastable phase compared to ZB, and its formation can be more favored in vigorous reaction conditions such as high temperature and with strongly coordinating surface ligands like alkyl phosphonic acids. Hence, a growth temperature

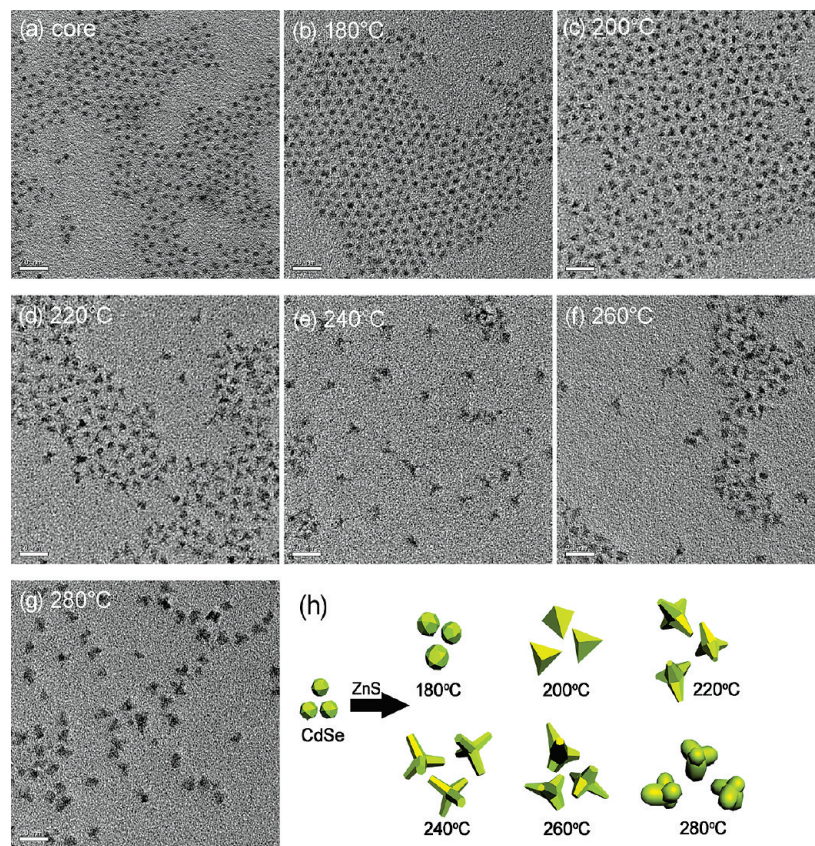


Figure 1. TEM images and structure illustration of CdSe core and CdSe/ZnS NCs with different ZnS growth temperatures: (a) CdSe core, and CdSe/ZnS NCs with ZnS shell grown at (b) 180, (c) 200, (d) 220, (e) 240, (f) 260, and (g) 280 °C; (h) schematic pictures of structural evolution. Scale bars in all the TEM images represent 20 nm.

of over 300 °C will benefit the formation of branched shell with WZ structure. But in this work, we find that the suitable temperature of preparing CdSe/ZnS with tetrapod-like shape is only 240 °C, and higher temperature can be destructive. A significant reason for this shape corruption is that fast interface diffusion and alloying between CdSe and ZnS occur at above 260 °C. We believe this alloying process drives the shell growth to a more homogeneous mode and flattens the ZnS arms. This interface alloying is further proved and discussed in the spectral analysis below.

Moreover in panels b and c of Figure 1 when the branched morphology has not formed yet, the particles are obviously smaller than those prepared at higher temperatures. Technically in the ZnS shell growth, precursor ions need to be absorbed to the particle surface to complete the shell growth. At low temperatures, the adsorption of precursor ions can be rather difficult, and it will cause insufficient growth of ZnS, and consequently lead to the smaller size of the final product.

The changes of crystal structure are investigated by powder XRD. From the diffraction patterns shown in Figure 2, the bottom curve for CdSe NCs well matches the reference of the bulk ZB-CdSe pattern (JCPDS file No. 88-2346) provided below, confirming their ZB crystal structure. After growing ZnS on CdSe, the XRD peaks shift to larger angle and match the bulk ZnS reference (JCPDS file No. 79-2204). But when ZnS grows at 180 °C, the peaks only exhibit a slight shift toward larger angle and sit between the reference patterns of bulk CdSe and ZnS. This means that the growth of ZnS here has considerably adopted the lattice parameters of CdSe core, implying that the ZnS shell is very thin, and this is in accordance

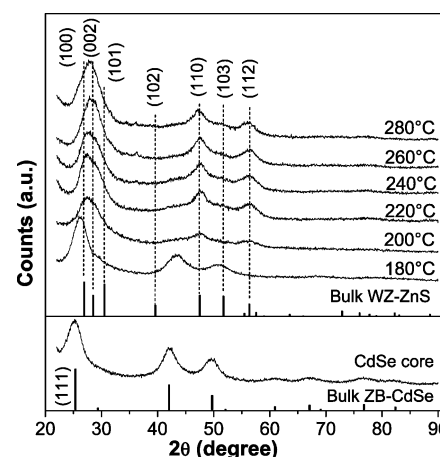


Figure 2. Powder XRD of CdSe core and CdSe/ZnS with ZnS grown from 180 to 280 °C. Reference XRD pattern of bulk ZB-CdSe and WZ-ZnS are provided correspondingly.

with the small particle size observed in Figure 1b. For the samples prepared at 200–280 °C, ZnS diffraction dominates, and the WZ structure could be deduced from the vague (103) peak, which appears like a slope at $2\theta = 51.7^\circ$. It is expected that ZnS grown at this temperature range has numerous defects such as stacking faults, because the formation of ZnS with WZ structure is rather difficult and usually needs an extremely high temperature, e.g., over 1000 °C.¹⁶ We consider the crystal defects result in the nontypical WZ-ZnS XRD patterns of these NCs, and HRTEM is performed to further investigate the structure.

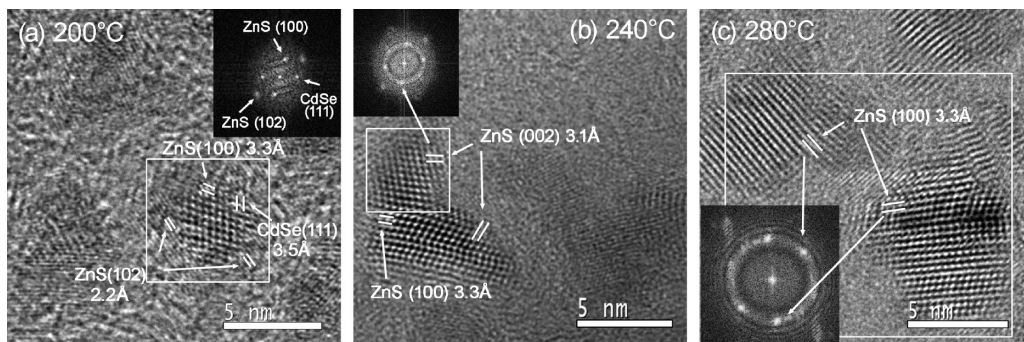


Figure 3. HRTEM images of CdSe/ZnS. Growth temperature of ZnS is 200 (a), 240 (b), and 280 °C (c). The 2D fast Fourier transform (FFT) patterns inserted in each image are obtained from the framed area, and the scale bars represent 5 nm.

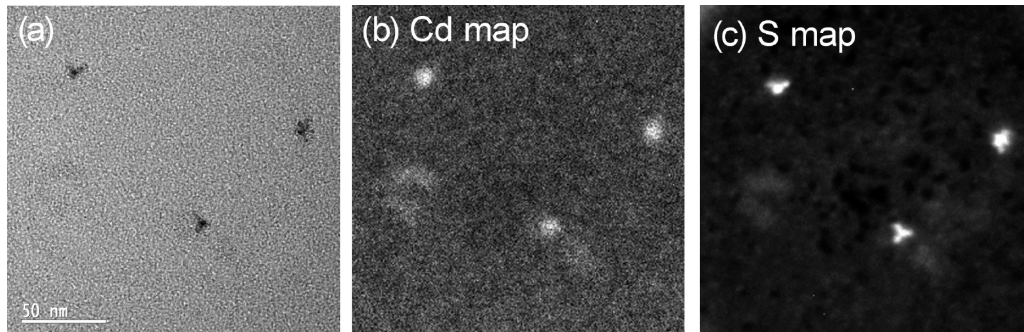


Figure 4. EELS elemental mapping of tetrapod-like CdSe/ZnS: (a) TEM bright field image, the scale bar represents 50 nm; (b) energy filtered cadmium elemental map; and (c) energy filtered sulfur elemental map.

HRTEM images are given in Figure 3. Figure 3a shows the near triangular NCs obtained at 200 °C, and the lattice fringes of both CdSe core and ZnS shell can be identified within one particle. As labeled in the image, the measured lattice *d*-spacing of 3.5 Å matches the (111) plane of ZB-CdSe, and the 3.3 Å spacing corresponds to the (100) plane of WZ-ZnS. Around the labeled particle there exist very light lattice fringes, which match the (102) plane of WZ-ZnS. In the branched CdSe/ZnS as shown in Figure 3b, the lattice *d*-spacing perpendicular to the *c*-axis of the ZnS arm is measured as 3.1 Å and fits the (002) plane of WZ-ZnS, while the 3.3 Å spacing at the center probably originates from the (100) plane of the upward ZnS arm. For the NCs shown in Figure 3c, however, the particle morphology is hard to define, and the main information from the crystal lattice is the (100) plane of WZ-ZnS. The HRTEM analysis further identifies the WZ structure of the ZnS shell in addition to the XRD results. It is worth noting that only Figure 3a shows the lattice of the CdSe core, and we speculate this is because the ZnS shell grown at 200 °C is not thick enough to cover the information from CdSe. When the shell gets thicker at higher temperatures, only ZnS will be seen under HRTEM.

Element distribution analysis of Cd and S in the tetrapod-like NCs was performed by energy filtered TEM of Cd M_{4,5}-edges at 404 eV and S L_{2,3}-edges at 165 eV. As shown in Figure 4, the elemental mappings of Cd and S represent the 2-dimensional distribution of CdSe and ZnS within the particles, and they show that Cd mainly resides in the particle center, while S spreads throughout a particle, which is in agreement with the design of seeded growth that CdSe serves as core and ZnS grows as covering shell. The vision of the S map is clear because S is more suitable for electron energy loss detection, while the Cd map is acquired under extended exposure time, and this may have caused the blurry edge of the Cd image.

Spectral properties of the NCs exhibit dramatic changes with reaction temperature variations, which are shown in Figure 5.

In Figure 5a, as the growth temperature of ZnS gets higher, the PL and absorption peaks first shift to the longer wavelength side and then shift backward. Figure 5b gives a clearer diagram of PL peak wavelengths, from which the peak shift reaches its maximum when ZnS grows at 220 °C, with a red shift of about 25 nm in respect to that of the CdSe core. Then at 240 °C, the red shift drops to 18 nm. Further raising the temperature to 260 °C, the red shift drops to 10 nm, but the TEM image in Figure 1f shows no decrease in particle size; thus the descent in the red shift could not be caused by the shrinkage of the particle. Since the shell material ZnS has a much wider band gap than CdSe and usually emits in the UV region, it seems that at higher temperature, interface alloying of CdSe and ZnS may have been triggered. This speculation is further demonstrated when ZnS grows at 280 °C, which shows an 11 nm blue shift in the PL peak compared to that of the CdSe core, while the sample obviously exhibits the biggest particle size as shown in Figure 1g. Therefore, it is certain that interface alloying between CdSe and ZnS indeed occurs at higher temperature. A luminescence illustration of excited samples is given in Figure 5c; the color of luminescence changes from yellow to orange and then to green as the temperature rises, which explains the wavelength shift of the PL peak clearly.

The alloying between different semiconductor materials in NCs has been mainly reported on spherical core/shell NCs with alloying temperature of over 270 °C,¹⁷ whereas only a few reports are on the interdiffusion and coalescence in anisotropic heterostructured NCs.¹⁸ From the above results, it is possible that alloying has already started at the interface even at 240 °C. Thus a detailed experiment was undertaken to find out more about the alloying process, and the results are given in Figure S2 in the Supporting Information, from which slight diffusion of Zn into CdSe is already seen at 240 and 220 °C by the blue shift of absorption spectra peaks. After S injection, the growth of the shell causes a red shift, but then a blue shift shows up

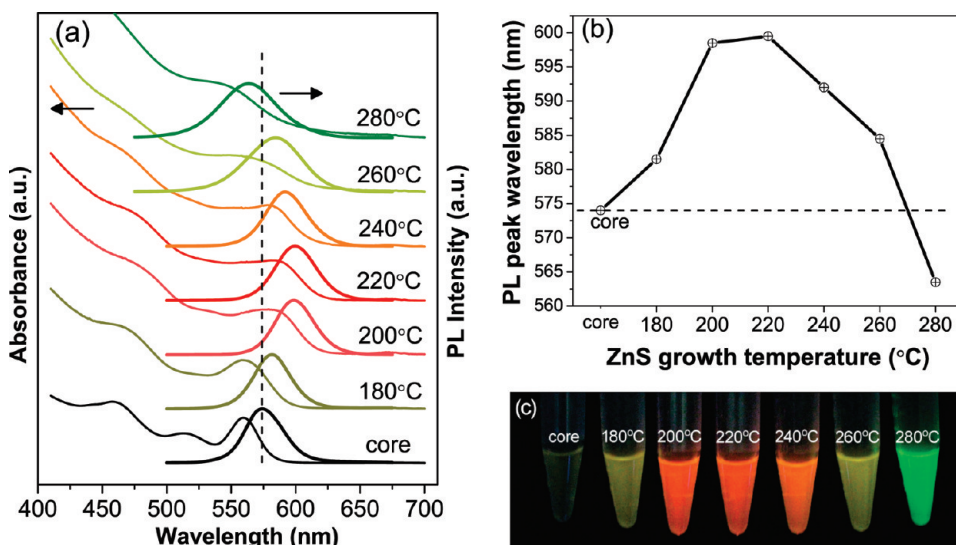


Figure 5. Spectral properties and luminescence of CdSe core and CdSe/ZnS NCs with different growth temperatures of ZnS: (a) UV-vis absorption and PL spectra; (b) a diagram of PL peak wavelengths; and (c) a photoillustration of samples excited with 365 nm UV irradiation.

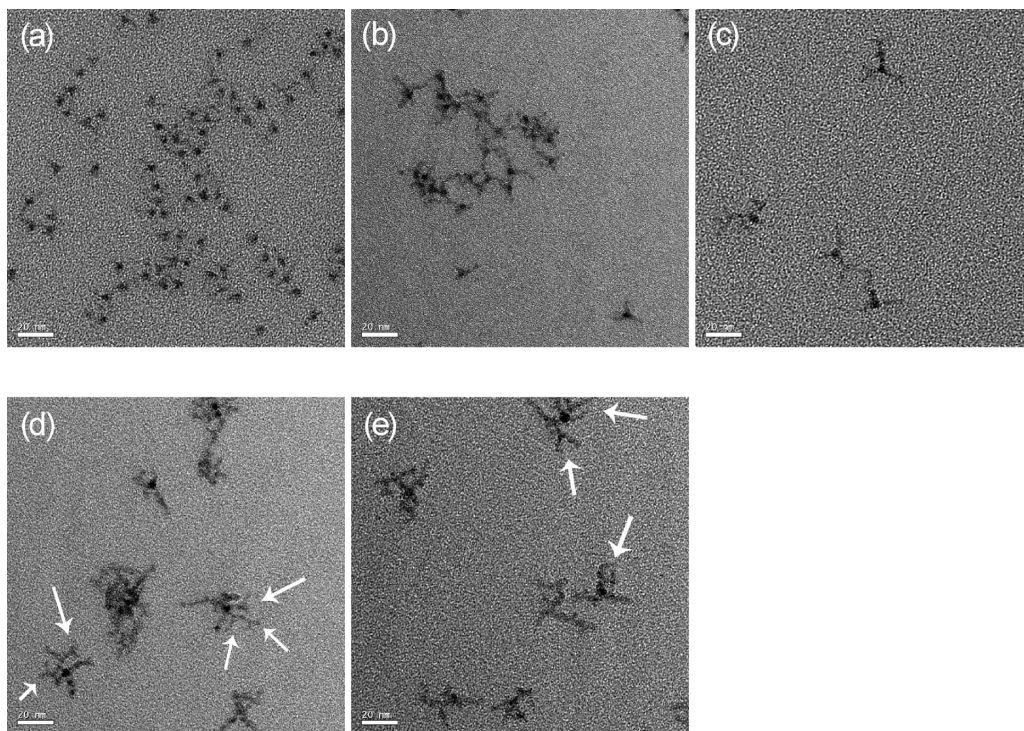


Figure 6. TEM images of CdSe/ZnS with different amounts of ZnS precursor injections. Denoted as designed monolayers of ZnS, the calculated thicknesses of the ZnS shell are (a) 4 MLs, (b) 6 MLs, (c) 8 MLs, (d) 12 MLs, and (e) 16 MLs. Scale bars represent 20 nm, and the arrows mark the places where ZnS grows with further branching.

again as the NCs are annealed, which manifests the occurrence of alloying even at lower temperatures. The reason that only higher temperature results in a distinct blue shift may be that, at lower temperature the diffusion rate is not fast enough to compensate the red shift induced by the thickening of the shell. It is noteworthy that in the process of shell growth at 260 and 280 °C, real time monitoring reveals that the luminescence color of NCs does not show a distinct change with Zn precursor injection, but a more pronounced blue shift is observed after injecting the S precursor, which means the migration of ions at high temperature is more likely to be simultaneous in both cation and anion.

3.2. Branched CdSe/ZnS NCs with Varying Amounts of ZnS Precursors.

We have presented the structural evolution of CdSe/ZnS, and the branched NCs are obtained at a moderate

reaction temperature range. In this study, structures and PL properties of the branched CdSe/ZnS are further investigated by varying the amount of ZnS precursor injections to grow the ZnS shell from 2 to 16 MLs. The temperature of ZnS growth is set at 240 °C, which is demonstrated above to be suitable for growing NCs with a tetrapod-like structure.

Morphologies of the CdSe/ZnS NCs with different amounts of ZnS precursor injections (denoted as monolayers of predetermined ZnS shells) are given in Figure 6. With 4 MLs of ZnS, the NCs show vague visions of branching; but when the ZnS shell increases to 6 MLs, ZnS arms become apparent and branching can be identified. Further increasing ZnS to 8 MLs, the NCs exhibit a tetrapod-like shape with the ZnS arm measuring about 10 nm. Then the particle structure becomes much more complicated when the shell reaches 12 and 16 MLs,

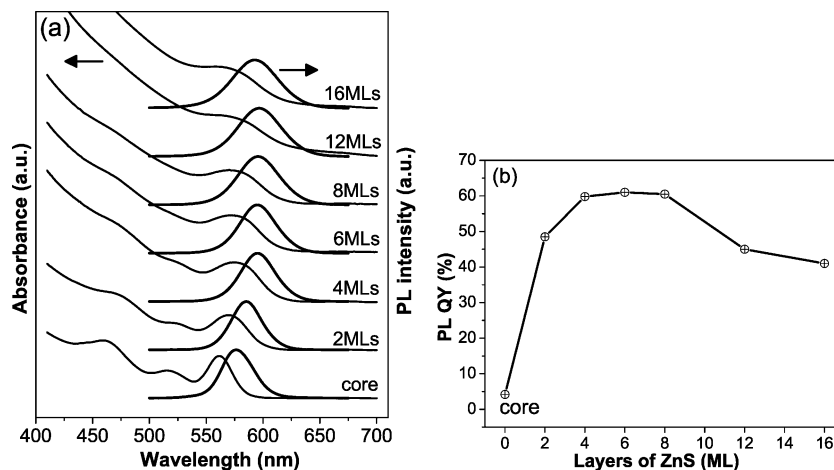


Figure 7. Optical spectra and quantum yield of CdSe and CdSe/ZnS with growing ZnS shell: (a) UV-vis absorption and PL spectra and (b) a diagram of photoluminescence quantum yield.

because the ZnS arms split in the middle and at the end, which is marked in panels d and e of Figure 6. Since the formation of the WZ crystal is usually facilitated at higher temperatures, we consider that under the relatively low temperature of 240 °C in our experiment, the growth of ZnS must be accompanied by considerable stacking faults and other defects, as well as accumulation of internal crystal strains. These faulty spots can induce growth of new ZnS arms, causing this multibranched morphology.

The absorption and PL spectra of these NCs are given in Figure 7a, from which we can see that the PL peak shifts to the longer wavelength side as ZnS deposits. But this red shift is only distinct when ZnS is of 2 and 4 MLs, further precursor injections do not continue this shifting trend. Combining with the particle structures in Figure 6, it can be concluded that the overall covering of ZnS around CdSe only occurs at the early stage of shell growth. Instead of thickening the shell, further additions of precursor mainly elongate the ZnS arms and generate splits.

A diagram of QY is provided in Figure 7b. The QY rises rapidly as CdSe is coated with a thin ZnS shell of only 2 MLs, and achieves saturation of about 60% when the shell reaches 4 MLs. Then the QY stays around 60% as ZnS grows from 4 to 8 MLs, and declines when ZnS arms get complicated with further branching. Analogous to the QY decrease of spherical core/shell NCs with thicker shell, for the branched CdSe/ZnS, as the ZnS arms grow, the multibranched structure indicates a non-negligible crystal strain, which will have negative impacts on the QY.

4. Conclusions

In conclusion, structural evolution and photoluminescence properties of ZB-CdSe-based CdSe/ZnS NCs are studied. The structure of the CdSe/ZnS NCs is found to be sensitive to the growth temperature of the ZnS shell. From 180 to 280 °C, the particle shape can be tuned from dot to near triangle and then to branched ones, including a tetrapod-like shape. Unlike other types of tetrapod NCs, the branched CdSe/ZnS is best synthesized at a moderate temperature of 240 °C, because high temperature can induce fast interface alloying between CdSe and ZnS, which will corrupt the branched structure and result in a distinct blue shift in the PL wavelength. Specifically for the tetrapod-like CdSe/ZnS NCs, the growth of ZnS first elongates the ZnS rods and then leads to further branching, and the quantum yield is found to decrease when the ZnS rods split.

Acknowledgment. This work was supported by the National Natural Science Foundation of China (NSFC, Nos. 10574047 and 20490210), the Hi-Tech Research and Development Program of China (the 863 program, No. 2007AA03Z312), the National Basic Research Program of China (the 973 program, No. 2006CB921606), and the Research Fund for the Doctoral Program of Higher Education (No. 20090142110064). The authors would also like to acknowledge the Analytical and Testing Center of HUST for TEM and XRD measurements, and Mr. Huoyang Xie in SMIC (Wuhan) Co. for HRTEM and EELS analysis.

Supporting Information Available: Supplementary description of experimental procedures, XPS measurement, experiment on the alloying process, additional XRD data, and TEM of CdSe/ZnS prepared without alkyl amine as surface ligand. This material is available free of charge via the Internet at <http://pubs.acs.org>.

References and Notes

- (a) Cozzoli, P. D.; Pellegrino, T.; Manna, L. *Synthesis, Properties and Perspectives of Hybrid Nanocrystal Structures*. *Chem. Soc. Rev.* **2006**, *35*, 1195–1208. (b) Talapin, D. V.; Mekis, I.; Goetzinger, S.; Kornowski, A.; Benson, O.; Weller, H. CdSe/CdS/ZnS and CdSe/ZnSe/ZnS Core-Shell-Shell Nanocrystals. *J. Phys. Chem. B* **2004**, *108*, 18826–18831. (c) Du, G. H.; Liu, Z. L.; Lu, Q. H.; Xia, X.; Jia, L. H.; Yao, K. L.; Chu, Q.; Zhang, S. M. Fe₃O₄/CdSe/ZnS Magnetic Fluorescent Bifunctional Nanocomposites. *Nanotechnology* **2006**, *17*, 2850–2854. (d) Ang, C. Y.; Giam, L.; Chan, Z. M.; Lin, A. W. H.; Gu, H.; Devlin, E.; Papaefthymiou, G. C.; Selvan, S. T.; Ying, J. Y. Facile Synthesis of Fe₂O₃ Nanocrystals Without Fe(CO)₅ Precursor and One-Pot Synthesis of Highly Fluorescent Fe₂O₃-CdSe Nanocomposites. *Adv. Mater.* **2009**, *21*, 869–873. (e) Nair, P. S.; Fritz, K. P.; Scholes, G. D. Evolutionary Shape Control During Colloidal Quantum-Dot Growth. *Small* **2007**, *3*, 481–487.
- (a) Shieh, F.; Saunders, A. E.; Korgel, B. A. General Shape Control of Colloidal CdS, CdSe, CdTe Quantum Rods and Quantum Rod Heterostructures. *J. Phys. Chem. B* **2005**, *109*, 8538–8542. (b) Carbone, L.; Nobile, C.; De Giorgi, M.; Della Sala, F.; Morello, G.; Pompa, P.; Hytch, M.; Snoeck, E.; Fiore, A.; Franchini, I. R.; Nadasan, M.; Silvestre, A. F.; Chiodo, L.; Kudera, S.; Cingolani, R.; Krahne, R.; Manna, L. Synthesis and Micrometer-Scale Assembly of Colloidal CdSe/CdS Nanorods Prepared by a Seeded Growth Approach. *Nano Lett.* **2007**, *7*, 2942–2950. (c) Deka, S.; Quarta, A.; Lupo, M. G.; Falqui, A.; Boninelli, S.; Giannini, C.; Morello, G.; De Giorgi, M.; Lanzani, G.; Spinella, C.; Cingolani, R.; Pellegrino, T.; Manna, L. CdSe/CdS/ZnS Double Shell Nanorods with High Photoluminescence Efficiency and Their Exploitation As Biolabeling Probes. *J. Am. Chem. Soc.* **2009**, *131*, 2948–2958. (d) Xi, L.; Boothroyd, C.; Lam, Y. M. Controlled Synthesis of CdTe and CdSe Multiblock Heteronanostructures. *Chem. Mater.* **2009**, *21*, 1465–1470.
- (a) Chen, W.; Chen, K.; Peng, Q.; Li, Y. Triangular CdS Nanocrystals: Rational Solvothermal Synthesis and Optical Studies. *Small* **2009**, *5*, 681–684. (b) Warner, J. H.; Tilley, R. D. Synthesis and

- Self-Assembly of Triangular and Hexagonal CdS Nanocrystals. *Adv. Mater.* **2005**, *17*, 2997–3001. (c) Cheng, Y.; Wang, Y.; Bao, F.; Chen, D. Shape Control of Monodisperse CdS Nanocrystals: Hexagon and Pyramid. *J. Phys. Chem. B* **2006**, *110*, 9448–9451.
- (4) (a) Liu, L.; Zhuang, Z.; Xie, T.; Wang, Y.-G.; Li, J.; Peng, Q.; Li, Y. Shape Control of CdSe Nanocrystals with Zinc Blende Structure. *J. Am. Chem. Soc.* **2009**, *131*, 16423–16429. (b) Cao, H.; Wang, G.; Zhang, S.; Zhang, X. Growth and Photoluminescence Properties of PbS Nanocubes. *Nanotechnology* **2006**, *17*, 3280–3287.
- (5) (a) Manna, L.; Milliron, D. J.; Meisel, A.; Scher, E. C.; Alivisatos, A. P. Controlled Growth of Tetrapod-Branched Inorganic Nanocrystals. *Nat. Mater.* **2003**, *2*, 382–385. (b) Cho, J. W.; Kim, H. S.; Kim, Y. J.; Jang, S. Y.; Park, J.; Kim, J.-G.; Kim, Y.-J.; Cha, E. H. Phase-Tuned Tetrapod-Shaped CdTe Nanocrystals by Ligand Effect. *Chem. Mater.* **2008**, *20*, 5600–5609. (c) Asokan, S.; Krueger, K. M.; Colvin, V. L.; Wong, M. S. Shape-Controlled Synthesis of CdSe Tetrapods Using Cationic Surfactant Ligands. *Small* **2007**, *3*, 1164–1169.
- (6) (a) Zhong, H.; Zhou, Y.; Yang, Y.; Yang, C.; Li, Y. Synthesis of Type II CdTe-CdSe Nanocrystal Heterostructured Multiple-Branched Rods and Their Photovoltaic Applications. *J. Phys. Chem. C* **2007**, *111*, 6538–6543. (b) McDaniel, H.; Shim, M. Size and Growth Rate Dependent Structural Diversification of Fe₃O₄/CdS Anisotropic Nanocrystal Heterostructures. *ACS Nano* **2009**, *3*, 434–440. (c) Milliron, D. J.; Hughes, S. M.; Cui, Y.; Manna, L.; Li, J.; Wang, L.-W.; Alivisatos, A. P. Colloidal Nanocrystal Heterostructures with Linear and Branched Topology. *Nature* **2004**, *430*, 190–195.
- (7) Talapin, D. V.; Nelson, J. H.; Shevchenko, E. V.; Aloni, S.; Sadtler, B.; Alivisatos, A. P. Seeded Growth of Highly Luminescent CdSe/CdS Nanoheterostructures with Rod and Tetrapod Morphologies. *Nano Lett.* **2007**, *7*, 2951–2959.
- (8) (a) Yu, W. W.; Wang, Y. A.; Peng, X. Formation and Stability of Size-, Shape-, and Structure-Controlled CdTe Nanocrystals: Ligand Effects on Monomers and Nanocrystals. *Chem. Mater.* **2003**, *15*, 4300–4308. (b) Manna, L.; Scher, E. C.; Alivisatos, A. P. Synthesis of Soluble and Processable Rod-, Arrow-, Teardrop-, and Tetrapod-Shaped CdSe Nanocrystals. *J. Am. Chem. Soc.* **2000**, *122*, 12700–12706.
- (9) (a) Xie, R.; Kolb, U.; Basche, T. Design and Synthesis of Colloidal Nanocrystal Heterostructures with Tetrapod Morphology. *Small* **2006**, *2*, 1454–1457. (b) Fiore, A.; Mastria, R.; Lupo, M. G.; Lanzani, G.; Giannini, C.; Carlino, E.; Morello, G.; De Giorgi, M.; Li, Y.; Cingolani, R.; Manna, L. Tetrapod-Shaped Colloidal Nanocrystals of II–VI Semiconductors Prepared by Seeded Growth. *J. Am. Chem. Soc.* **2009**, *131*, 2274–2282.
- (10) Zhou, Y.; Li, Y.; Zhong, H.; Hou, J.; Ding, Y.; Yang, C.; Li, Y. Hybrid Nanocrystal/Polymer Solar Cells Based on Tetrapod-Shaped CdSe_xTe_{1-x} Nanocrystals. *Nanotechnology* **2006**, *17*, 4041–4047.
- (11) Zhong, H.; Scholes, G. D. Shape Tuning of Type II CdTe-CdSe Colloidal Nanocrystal Heterostructures through Seeded Growth. *J. Am. Chem. Soc.* **2009**, *131*, 9170–9171.
- (12) Zhai, T.; Dong, Y.; Wang, Y.; Cao, Z.; Ma, Y.; Fu, H.; Yao, J. Size-Tunable Synthesis of Tetrapod-Like ZnS Nanopods by Seed-Epitaxial Metal-Organic Chemical Vapor Deposition. *J. Solid State Chem.* **2008**, *181*, 950–956.
- (13) (a) Yang, Y. A.; Wu, H.; Williams, K. R.; Cao, Y. C. Synthesis of CdSe and CdTe Nanocrystals Without Precursor Injection. *Angew. Chem., Int. Ed.* **2005**, *44*, 6712–6715. (b) Lim, S. J.; Chon, B.; Joo, T.; Shin, S. K. Synthesis and Characterization of Zinc-Blende CdSe-Based Core/Shell Nanocrystals and Their Luminescence in Water. *J. Phys. Chem. C* **2008**, *112*, 1744–1747.
- (14) (a) Li, J. J.; Wang, Y. A.; Guo, W.; Keay, J. C.; Mishima, T. D.; Johnson, M. B.; Peng, X. Large-Scale Synthesis of Nearly Monodisperse CdSe/CdS Core/Shell Nanocrystals Using Air-Stable Reagents via Successive Ion Layer Adsorption and Reaction. *J. Am. Chem. Soc.* **2003**, *125*, 12567–12575. (b) Xie, R.; Kolb, U.; Li, J.; Basche, T.; Mews, A. Synthesis and Characterization of Highly Luminescent CdSe-Core CdS/Zn_{0.5}Cd_{0.5}S/ZnS Multishell Nanocrystals. *J. Am. Chem. Soc.* **2005**, *127*, 7480–7488.
- (15) Fery-Forgues, S.; Lavabre, D. Are Fluorescence Quantum Yields So Tricky to Measure? A Demonstration Using Familiar Stationery Products. *J. Chem. Educ.* **1999**, *76*, 1260–1264.
- (16) Yin, L.-W.; Bando, Y.; Zhan, J.-H.; Li, M.-S.; Golberg, D. Self-Assembled Highly Faceted Wurtzite-Type ZnS Single-Crystalline Nanotubes with Hexagonal Cross-Sections. *Adv. Mater.* **2005**, *17*, 1972–1977.
- (17) (a) Zhong, X.; Han, M.; Dong, Z.; White, T. J.; Knoll, W. Composition-Tunable Zn_xCd_{1-x}Se Nanocrystals with High Luminescence and Stability. *J. Am. Chem. Soc.* **2003**, *125*, 8589–8594. (b) Zhong, X.; Zhang, Z.; Liu, S.; Han, M.; Knoll, W. Embryonic Nuclei-Induced Alloying Process for the Reproducible Synthesis of Blue-Emitting Zn_xCd_{1-x}Se Nanocrystals with Long-Time Thermal Stability in Size Distribution and Emission Wavelength. *J. Phys. Chem. B* **2004**, *108*, 15552–15559. (c) Protiere, M.; Reiss, P. Highly Luminescent Cd_{1-x}Zn_xSe/ZnS Core/Shell Nanocrystals Emitting in the Blue-Green Spectral Range. *Small* **2007**, *3*, 399–403. (d) Jun, S.; Jang, E. Interfused Semiconductor Nanocrystals: Brilliant Blue Photoluminescence and Electroluminescence. *Chem. Commun.* **2005**, 4616–4618.
- (18) Koo, B.; Korgel, B. A. Coalescence and Interface Diffusion in Linear CdTe/CdSe/CdTe Heterojunction Nanorods. *Nano Lett.* **2008**, *8*, 2490–2496.

JP100442V

Supporting Information

Structural Evolution and Photoluminescence of Zinc-Blende CdSe-Based CdSe/ZnS Nanocrystals

Xing Xia, Zuli Liu, Guihuan Du, Yuebin Li and Ming Ma*

School of Physics, Huazhong University of Science and Technology, 1037 Luoyu
Road, Wuhan 430074, People's Republic of China.

1. Supplementary experimental procedures

1.1. Preparation of stock solutions

Three stock solutions containing 0.1 mol/liter (0.1 M) of Cd, Zn, and S, respectively, were prepared before the experiments.

For Cd solution, 5 mmol of CdO powder, 14.1 mL of oleic acid (OA, with purity of ~90%, and molar ratio of Cd:OA=1:8) and 35.9 mL of 1-octadecene (ODE) were loaded into a three-neck-flask. The flask was heated to 120 °C, pumped to remove air and flushed with argon. Then it was heated to 280-300 °C directly to generate a transparent light yellow solution. When the liquid cooled down to 120 °C, the flask was repeatedly pumped to remove moisture, and then the solution was further cooled to 50 °C, bottled with argon filling and stored at 4 °C.

Zn solution was prepared accordingly, with 5 mmol of ZnO powder instead, and 14.1 mL of OA and 35.9 mL of ODE. The reaction temperature was set at ~300 °C to generate a slightly yellow solution.

S solution was prepared by dissolving 5 mmol of sulfur powder with 50 mL of ODE at ~200 °C; the final product was light amber-colored liquid.

1.2. Purification of NCs

The NCs were purified by extraction with hexane/methanol for at least 3-5 times. Specifically, 5 mL of hexane was added to the crude NCs solution at ~50 °C and mixed, followed by addition of 10-20 mL of methanol. The liquid was sealed and mixed by shaking, and it would separate into two phases after standing still for a while, and then the lower methanol phase was removed. Sometimes a few extra drops of hexane could help to accelerate the phase separation. In order to effectively remove the excessive stearic acid or octadecylamine, the extraction process was performed at 60-70 °C, but higher temperature might induce poor solubility of the final product.

Purified NCs were precipitated by centrifugation with addition of acetone, and they were dried under vacuum at ~50 °C. The final product was dispersed in hexane or chloroform for further purpose.

1.3. Calculation of precursors

The diameter and quantity of CdSe particles were measured and calculated according to Yu et al.¹ It should be pointed out that if stearic acid is not effectively cleaned, the CdSe solution will appear a bit cloudy and a strong background scattering will affect the accuracy of absorbance measurement. In this case the CdSe NCs should be dispersed in hexane and subject to centrifugation before measurement. With this process, stearic acid will precipitate and the solution can be optically clear for further characterization.

The calculation of shell precursor was based on bulk lattice parameters of ZB-CdSe ($a=b=c=6.05 \text{ \AA}$) and ZB-ZnS ($a=b=c=5.41 \text{ \AA}$), assuming that particle surface consists of equal cations and anions and the particle is spherical. So each surface 2D unit cell will contain one cation and one anion. Regardless of the final shape, the amount of surface cation/anion can be approximately calculated as $4\pi r^2/d^2$, of which r is the radius of the core and d is the corresponding lattice parameter of substrate material. For example, to grow ZnS on $1 \times 10^{-4} \text{ mmol}$ of CdSe cores with 3.3 nm in diameter, the amount of 0.1 M Zn and S precursor solution needed is ~93 μl each for the first monolayer of ZnS, and this will increase the particle radius by 0.31 nm (the thickness of one monolayer of ZnS is 0.31 nm.²), thus the second monolayer will need an injection of ~0.17 mL, and accordingly, the third and fourth injection will be 0.22 mL and 0.29 mL respectively.

2. X-ray Photoelectron Spectroscopy (XPS) analysis

XPS was adopted for surface analysis of CdSe core and tetrapod-like CdSe/ZnS NCs prepared at 240 °C on a VG MultiLab 2000 X-ray Photoelectron Spectrometer (Thermo Fisher Scientific). From Figure S1, with the coverage of ZnS, the photoelectron emission from CdSe core is greatly weakened, and instead, Zn and S emission dominates, indicating the growth of ZnS shell on CdSe core. The surface elemental ratio from XPS is given in Table S1, which shows that most atoms on the surface are carbon and oxygen from the organic surface ligands, and the semiconductor material is covered underneath, with a change in surface atom ratio of Cd, Se, Zn and S after the growth of ZnS.

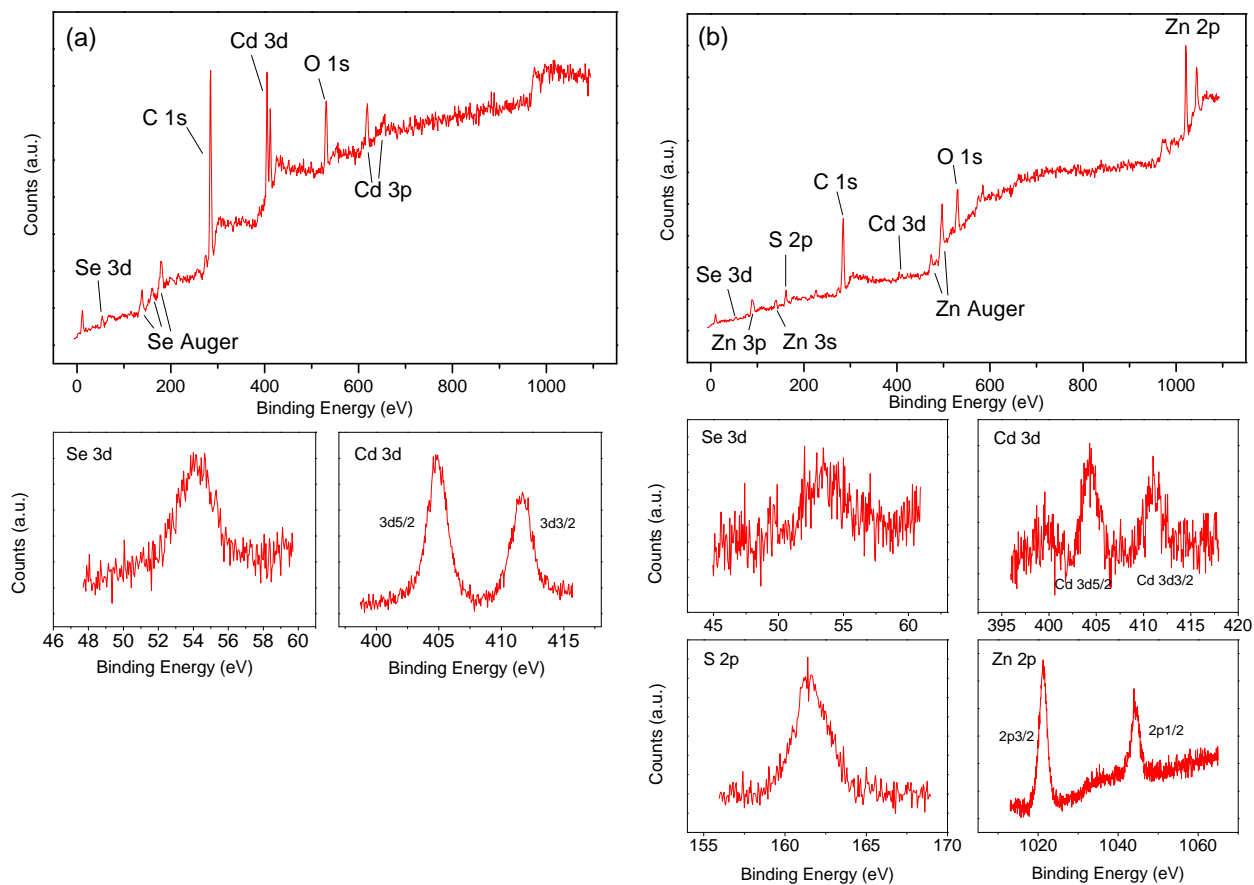


Figure S1. (a) Wide scan XPS spectrum of ZB-CdSe, lower insets are the expanded scan of Se 3d and Cd 3d peaks; (b) wide scan XPS spectrum of tetrapod-like CdSe/ZnS prepared at 240 °C, lower insets are the expanded scan of Se 3d, Cd 3d, S 2p, and Zn 2p peaks.

Table S1. Calculated surface elemental ratio of CdSe and CdSe/ZnS from the XPS spectra.

Element	CdSe core Atom %	CdSe/ZnS tetrapod Atom %
C	78.77	66.32
O	14.52	17.21
Cd	4.2	0.75
Se	2.51	1.92
Zn	-	5.77
S	-	8.02

3. Alloying of CdSe and ZnS

From Figure 5 in the article, we can tell that alloying of CdSe and ZnS is evident at 260 and 280 °C, but it is hard to define this at 240 °C. According to the relationship between absorption/emission and diameter of CdSe reported by Yu et al.,¹ 10-20 nm shift in the wavelength of absorption/emission peak can be induced by only a few angstroms of change in particle size. Thus it would be extremely hard to identify interface diffusion through distinct views of elemental distribution. So in this study, shift in absorption wavelength is adopted for analysis of interface diffusion. In order to avoid red shift caused by shell growth as much as possible, only one monolayer of ZnS (~0.31 nm) is designed to grow on CdSe, and the NCs were annealed to promote interface alloying.

In the ZnS shell growth procedure by SILAR, Zn precursor is first injected and the NCs are incubated at certain temperature, and then S precursor is introduced to generate ZnS shell. Shown in Figure S2, after incubating CdSe core with Zn ion at 220 and 240 °C for 15 min, a blue shift is seen in the first absorption peak. With the following S injection, absorption peak shows drastic red shift as ZnS shell generates, and then exhibits blue shift in the annealing process. From Figure S2, it can be concluded that even at 220 and 240 °C, surface and interface alloying still exists.

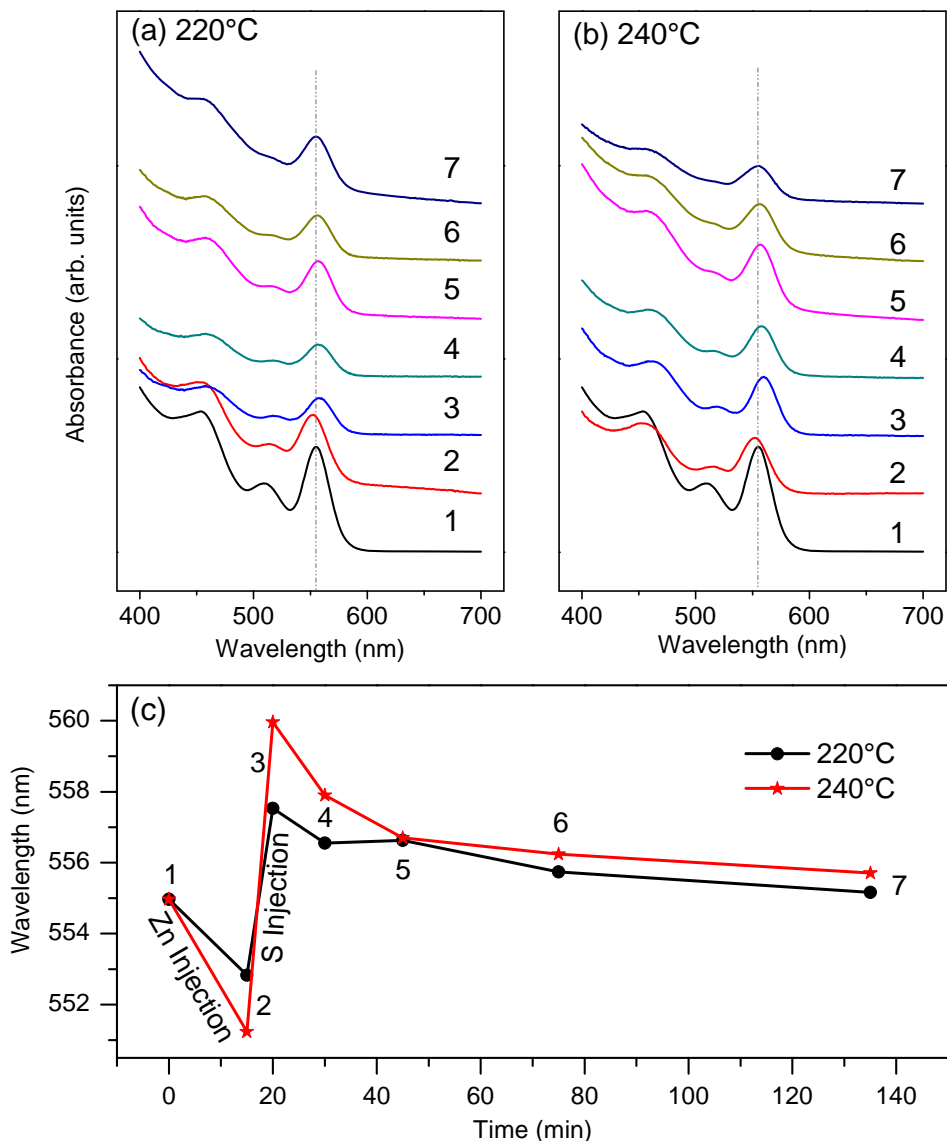


Figure S2. UV-vis absorption of CdSe core and CdSe/ZnS as a temporal evolution of ZnS growth at different temperature, (a) 220 °C and (b) 240 °C; (c) plots of the absorption peaks related to the reaction time; the numbers 1 to 7 represent (1): CdSe core, (2): 15 min after Zn injection, (3): 5 min after S injection, (4): 15 min after S injection, (5): 30 min after S injection, (6): 60 min after S injection, and (7): 120 min after S injection.

4. CdSe/ZnS grown without octadecylamine

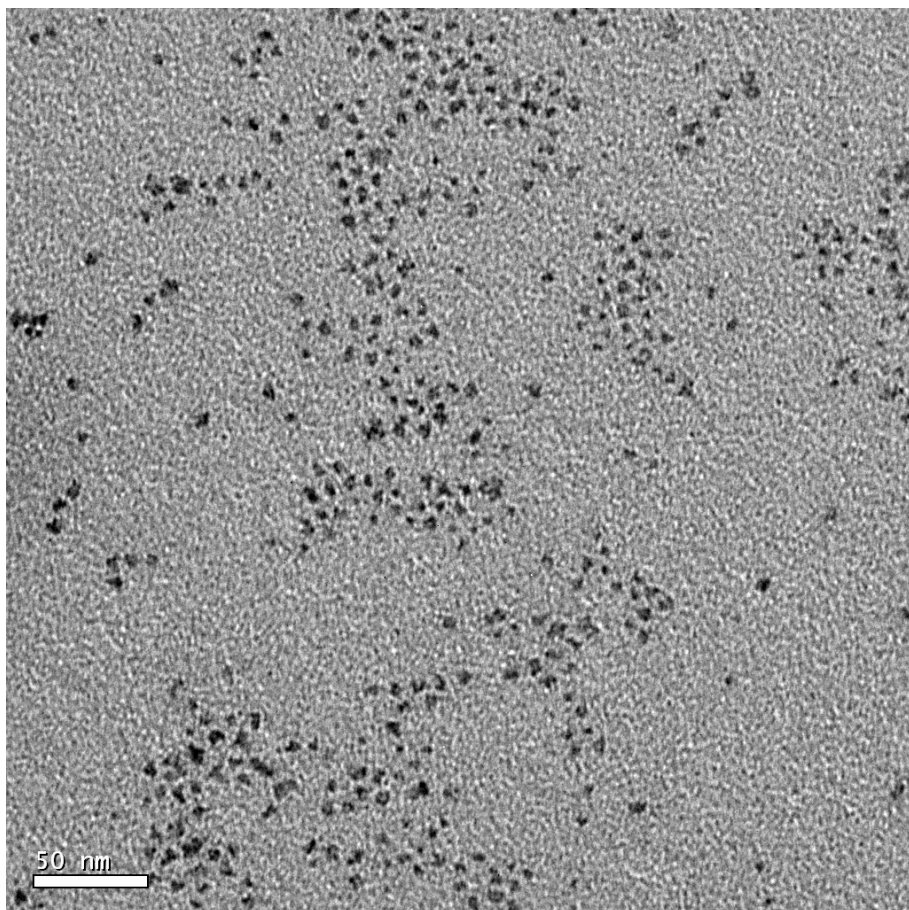


Figure S3. TEM image of CdSe/ZnS synthesized at 240 °C; ZnS was grown in the absence of octadecylamine.

In order to exam the effect of alkyl amine in the formation of branched CdSe/ZnS, a control experiment was carried out for contrast, in which the reaction condition is identical to that of the tetrapod-like NCs shown in Figure 1e, only except that the alkyl amine ligand octadecylamine was unused.

The resulting nanocrystals show irregular “dot” shape as presented in Figure S3. This manifests that surface ligand molecules are crucial to the formation of branched ZnS shell. The possible mechanism is that, octadecylamine molecules selectively adhere to the surface planes perpendicular to the *c*-axis of WZ crystal, restricting their growth and promoting the growth of ZnS along *c*-axis.³ This function of octadecylamine is

identical to that of alkyl phosphonic acid in promoting the formation of nano rods and tetrapods.

5. XRD of branched CdSe/ZnS with increasing ZnS shell

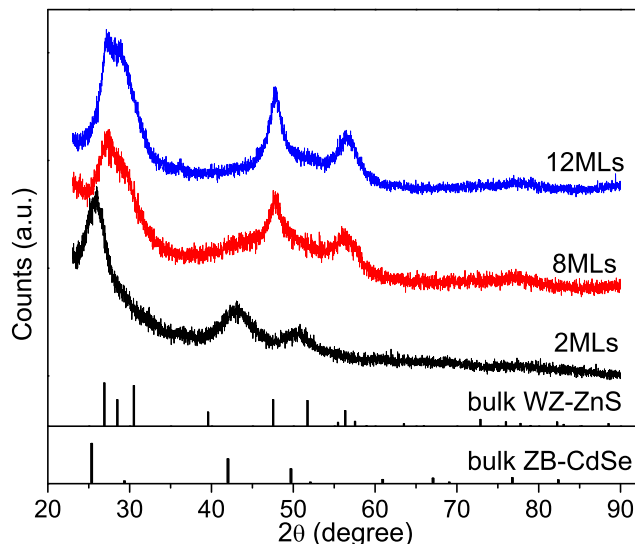


Figure S4. Powder XRD patterns of branched CdSe/ZnS NCs with different layers of ZnS. The reference XRD patterns in the bottom correspond to bulk material of zinc-blende (ZB) CdSe (JCPDS No. 88-2346) and wurtzite (WZ) ZnS (JCPDS No. 79-2204).

References

- [1] Yu, W. W.; Qu, L.; Guo, W.; Peng, X. Experimental Determination of the Extinction Coefficient of CdTe, CdSe, and CdS Nanocrystals. *Chem. Mater.* **2003**, *15*, 2854-2860.
- [2] Xie, R.; Kolb, U.; Li, J.; Basche, T.; Mews, A. Synthesis and Characterization of Highly Luminescent CdSe-Core CdS/ $Zn_{0.5}Cd_{0.5}S$ /ZnS Multishell Nanocrystals. *J. Am. Chem. Soc.* **2005**, *127*, 7480-7488.
- [3] Cozzoli, P. D.; Pellegrino, T.; Manna, L. Synthesis, Properties and Perspectives of Hybrid Nanocrystal Structures. *Chem. Soc. Rev.* **2006**, *35*, 1195-1208.